Lawrence Berkeley National Laboratory

LBL Publications

Title

High On/Off Ratio Memristive Switching of Manganite/Cuprate Bilayer by Interfacial Magnetoelectricity

Permalink

https://escholarship.org/uc/item/58d462p5

Journal

Advanced Materials Interfaces, 3(16)

ISSN

2196-7350

Authors

Shen, Xiao
Pennycook, Timothy J
Hernandez-Martin, David
et al.

Publication Date

2016-08-01

DOI

10.1002/admi.201600086

Peer reviewed

eScholarship.org Powered by the California Digital Library
University of California

High On/Off Ratio Memristive Switching of Manganite/Cuprate Bilayer by Interfacial Magnetoelectricity

Xiao Shen, Timothy J. Pennycook, David Hernandez-Martin, Ana Pérez, Yevgeniy S. Puzyrev, Yaohua Liu, Suzanne G. E. te Velthuis, John W. Freeland, Padraic Shafer, Chenhui Zhu, Maria Varela, Carlos Leon, Zouhair Sefrioui, Jacobo Santamaria, and Sokrates T. Pantelides*

Memristive switching serves as the basis for a new generation of electronic devices. Conventional memristors are two-terminal devices in which the current is turned on and off by redistributing point defects, e.g., vacancies. Memristors based on alternative mechanisms have been explored, but achieving both high on/off ratio and low switching energy, as needed in applications, remains a challenge. This study reports memristive switching in $La_{0.7}Ca_{0.3}MnO_3/PrBa_2Cu_3O_7$ bilayers with an on/off ratio greater than 10^3 and results of density functional theory calculations in terms of which it is concluded that the phenomenon is likely the result of a new type of interfacial magnetoelectricity. More specifically, this study shows that an external electric field induces subtle displacements of the interfacial Mn ions, which switches on/off an interfacial magnetic "dead layer", resulting in memristive behavior for spin-polarized electron transport across the bilayer. The interfacial nature of the switching entails low energy cost, about of a tenth of atto Joule for writing/erasing a "bit". The results indicate new opportunities for manganite/cuprate systems and other transition metal oxide junctions in memristive applications.

1. Introduction

The transistor, a three-terminal device, is the basic unit in modern electronics, which powers information technology. Driven by the approaching limits of transistor scaling, interest in exploring memristors as an alternative has recently surged. Memristors are devices in which the passage of current is controlled by exploiting the defining property of memristive materials, namely a pinched current–voltage hysteresis loop.[1,2] In a transistor, the different conducting states are achieved by altering the gate voltage that externally modulates the carrier density in the semiconductor. In a memristor, one uses an external means to generate different conducting states by inducing reversible atomic displacements.

Prof. X. Shen, Dr. Y. S. Puzyrev, Prof. S. T. Pantelides
Department of Physics and Astronomy
Vanderbilt University
Nashville, TN 37235, USA

Prof. X. Shen
Department of Physics and Materials Science
University of Memphis
Memphis, TN 38152, USA
E-mail: xshen1@memphis.edu

Dr. T. J. Pennycook
SuperSTEM Laboratory
Daresbury WA4 4AD, UK

Dr. T. J. Pennycook
Department of Materials
Oxford University
Parks Road, Oxford OX1 3PH, UK

Dr. D. Hernandez-Martin, A. Pérez, Prof. M. Varela, Prof. C. Leon, Prof. Z. Sefrioui, Prof. J. Santamaria
Grupo de Fisica de Materiales Complejos
Universidad Complutense
28040 Madrid, Spain

Dr. Y. Liu
Quantum Condensed Matter Division
Oak Ridge National Laboratory
Oak Ridge, TN 37831, USA

Dr. Y. Liu, Dr. S. G. E. te Velthuis
Materials Science Division
Argonne National Laboratory
Argonne, IL 60439, USA

Dr. J. W. Freeland
Advanced Photon Source
Argonne National Laboratory
Argonne, IL 60439, USA

Dr. P. Shafer, Dr. C. Zhu
Advanced Light Source
Lawrence Berkeley National Laboratory
Berkeley, CA 94720, USA

Prof. M. Varela, Prof. S. T. Pantelides
Materials Science and Technology Division
Oak Ridge National Laboratory
Oak Ridge, TN 37831, USA

Prof. J. Santamaria
Instituto de Magnetismo Aplicado
Universidad Complutense
28040 Madrid, Spain

Prof. S. T. Pantelides
Department of Electrical Engineering and Computer Science
Vanderbilt University
Nashville, TN 37235, USA

DOI: 10.1002/admi.201600086

© 2016 WILEY-VCH Verlag GmbH & Co. KGaA, Weinheim

Memristors often have the additional property of continuous tunability, which emulates biological synapses.[3,4]

Many materials have been explored for their memristive behavior. The most widely studied types are based on the dynamics of defects such as oxygen vacancies or metal ions.[5–7] Different resistance states are generated by either causing the formation and rupture of a conductive filament or modifying the Schottky barrier at the contacts. High on/off ratios (>10^3) are often achieved.[8,9] Memristors based on other switching mechanisms have also been demonstrated, including molecular memristors,[10] ferroelectric memristors,[11] and spin-transfer torques.[12] These memristors typically have on/off ratio smaller than 10^2 with the exception of ferroelectric memristors, which can reach 10^4.[13] Several recent papers demonstrated that the magnetic polarization in magnetic tunnel junctions (MTJs)[14] and magnetic-metal/ferroelectric junctions[15–17] can be modified by external electric fields, effectively producing memristive behavior, but the on/off ratio is typically smaller than 10.

In this paper we report memristive switching with high on/off ratio in transition metal oxide (TMO) interfaces and show that it is unlikely to involve defect motion. Instead, it is more likely that the phenomenon arises from a new type of interfacial magnetoelectricity. We demonstrate experimentally that the resistance of $La_{0.7}Ca_{0.3}MnO_3$ (LCMO)/$PrBa_2Cu_3O_7$ (PBCO) bilayers can be changed 10^3-fold by an external electric field. The switching can happen at temperatures as low as 50 K, whereby the underlying mechanism is unlikely to be oxygen-vacancy diffusion. Although other explanations may be possible, we report results of density functional theory (DFT) calculations in terms of which we conclude that the memristive behavior originates from the switching of a "magnetic dead layer" (MDL) at the LCMO/PBCO interface by the external electric field. An MDL can exist at the interface of ferromagnetic (FM) and non-ferromagnetic TMOs such as $La_{0.67}Ca_{0.33}MnO_3$/$YBa_2Cu_3O_7$, where the first layer of the FM TMO can be antiferromagnetically (AFM) coupled to bulk FM TMO.[18] Results from first-principles calculations show that the external electric field induces subtle displacements of the interfacial Mn atoms and such displacements control the presence or absence of an MDL, which causes the memristive behavior for the transport of spin-polarized electrons. The subtle nature of the switching makes the system very energy efficient (≈0.1 atto Joule to write/erase a bit). The high on/off ratio, non-defect based mechanism, and the low switching energy make the LCMO/PBCO bilayer and similar manganite/cuprate systems particularly attractive for memristive devices.

2 Results and Discussions

$La_{0.7}Ca_{0.3}MnO_3$/$PrBa_2Cu_3O_7$ bilayers were grown using a high pressure (3.4 mbar) pure oxygen sputtering technique at elevated temperature (900 °C), which is known to yield good epitaxial properties.[19] Standard optical lithography and ion milling by a plasma source or electrically SiO_2 isolated mesas were used to define square micrometer size (4 × 4 μm^2) pillars to measure perpendicular transport. The top electrode was evaporated silver. Transport (resistance versus field loops and *I*–*V* curves) was measured in a closed-cycle He cryostat equipped with an electromagnet that supplies a magnetic field up to 4000 Oe. For all measurements, the top contact was grounded.

Aberration-corrected scanning transmission electron microscopy (STEM) was employed to determine the atomic scale structure and composition of the LCMO/PBCO bilayer. High-angle annular dark field (HAADF) imaging shows that the layers grow coherently on the STO substrate as seen in **Figure 1**b. The atomic-number contrast (Z contrast) of HAADF imaging allows the STO, LCMO, and PBCO layers to be easily identified. However, because La, Pr, and Ba are similarly heavy elements compared to the similarly light Cu and Mn elements the termination of the interface is not clear from the HAADF images alone. Atomic-resolution spectrum imaging was therefore performed using electron-energy-loss spectroscopy, which is included in the Supporting Information. The maps show that the interface consists of a Mn-rich plane terminating the LCMO, adjacent to a single Ba-rich plane terminating the PBCO. We therefore assume an MnO_2-BaO termination at the interface in our atomistic model below.

Electrical measurements in the current-perpendicular-to-plane geometry reveal a memristive hysteresis of the LCMO/PBCO bilayer, as shown in the current–voltage relation in Figure 1c. Figure 1d shows the resistance hysteresis of the junction that was read with a voltage of 200 mV at 100 K. Under an external magnetic field of 4 kOe, the resistance (R) of the as-fabricated bilayer junction is around 300 000 Ω. By applying negative biases greater than −0.5 V, the measured resistance can be increased by more than three orders of magnitude, with larger maximum biases resulting in greater *R* values. Applying a reverse positive bias switches the bilayer back to the initial low-resistance state. Such a large magnitude of resistance change is not observed in LCMO/PBCO/LCMO trilayer samples, which instead show a smaller factor-two change in resistance.[20] The resistance hysteresis varies with both temperature and magnetic field. The hysteresis window narrows as the temperature increases and vanishes when the temperature is raised to 180 K, which is above the Curie temperature of LCMO films (155 K), as shown in Figure 1e. The T_C of the film is lower than the bulk value of ≈240 K, which probably is due to the strain effect on the very thin film. X-ray magnetic circular dichroism (XMCD) measurements were carried out, showing that there is exchange coupling between the interfacial Cu and Mn moments. The results are included in the Supporting Information. The lack of hysteresis above Curie temperature suggests that hysteresis is related to the spin-polarization of the current. Meanwhile, the hysteresis window widens as the magnetic field increases, with stronger magnetic fields yielding greater resistance at the high-resistance state (Figure 1f). However, the switching can happen without using an external magnetic field. This feature distinguishes the LCMO/PBCO system from other heterostructure systems that use the spin-filtering effect, such as quasimagnetic tunnel junctions (QMTJ), which are switched by magnetic fields.[21]

The memristive behavior of TMO films is often attributed to the diffusion of oxygen vacancies.[4,5,7,22,23] This mechanism has also been invoked in the case of TMO bilayer and trilayer structures such as PCMO/YBCO junctions.[24] A role of oxygen vacancies in the switching cannot be ruled out. However, there

© 2016 WILEY-VCH Verlag GmbH & Co. KGaA, Weinheim

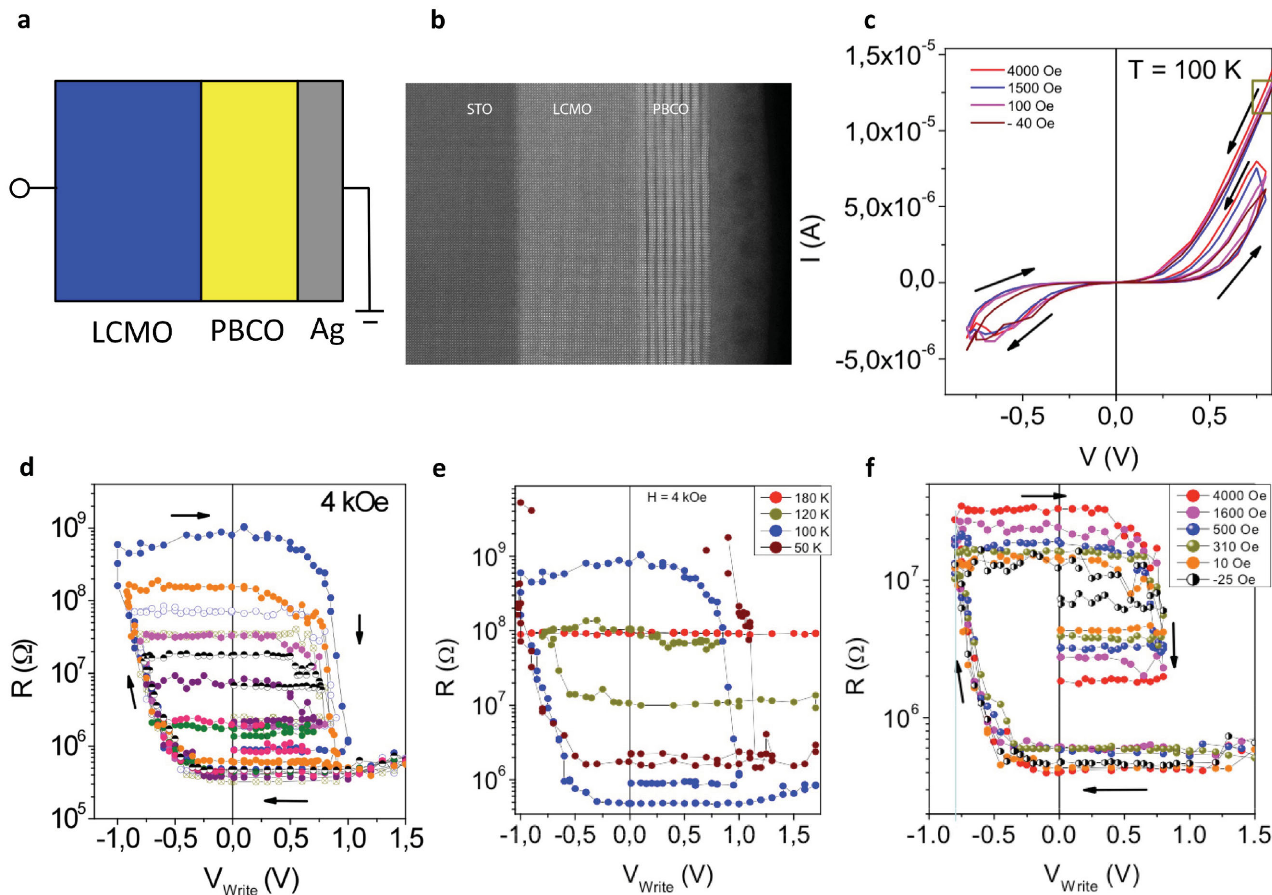

Figure 1. a) The layout of the bilayer structure, where the top electrode (grounded) is shown in the right. b) HAADF image of the LCMO/PBCO sample. c) *I–V* hysteresis of the LCMO/PBCO bilayer recorded at 100 K. d) Resistance hysteresis at 100 K. The different colors correspond to measurements with different maximum negative voltages. e) Temperature dependence of the resistance hysteresis. f) Magnetic field dependence of the resistance hysteresis.

are several factors that suggest a different mechanism may be at play. First, we observe memristive hysteresis when the temperature is far below room temperature, meaning there may not be sufficient thermal energy to enable the vacancy motion despite the barrier being lowered by the external electric field.[4,5,7,25] More specifically, the diffusion barrier for oxygen-vacancy migration in LCMO is 1.3 eV[26] and the estimated maximum electric field during the experiment is 0.04 V Å^{-1} for a 1 V bias. For a hopping distance of 2 Å, the barrier lowering effect due to the electric field is 0.04 eV. For such an amount of barrier lowering, the diffusivity increases non-linearly with the electric field.[4,25] However the overall diffusivity is still too low for vacancy migration. Even if we use a generously overestimated value of 0.1 eV for the diffusion barrier lowering, the resulting diffusion barrier is still 1.2 eV.

Although a diffusion barrier ≈1 eV allows detectable vacancy motion at room temperature,[27] such a barrier is quite large for diffusion at 100 K, as a 1 eV barrier at 100 K is equivalent to a 3 eV barrier at 300 K for diffusivity. Furthermore, if the motion of oxygen vacancies is causing the switching, the switching voltage should decrease as the temperature increases. The data do not show any such effect. In Figure 1e we see that, on the left, all three temperatures show a switch occurring at about –0.6 V and on the right the switch is at about +0.9 V for all temperatures.

The possibility that Joule heating might raise the temperature of the device to allow vacancy migration can be ruled out. First, junctions with different areas carved out of the same sample showed current levels that scale approximately with junction area, (Figure S4, Supporting Information). These data indicate that the current flow is homogeneous and exclude Joule heating at filaments. The possibility that Joule heating in the entire device causes vacancy migration is also not very likely for the following reasons: If Joule heating were sufficient for oxygen vacancies to move by overcoming a barrier of 1.3 eV, the temperature in the active region would be at or above room temperature, which is much higher than the Curie temperature of LCMO. As a result, the LCMO would undergo a phase transition and lose its magnetization, and the resistance hysteresis would not occur at all, contrary to observations, which find hysteresis, but only up to the Curie temperature. (We can rule out the possibility of quick cool down between current measurement and set/reset. Such quick cool down only happens in cases of very fast switching when the current reaches a compliance value. Although we used current compliance, the current never reaches compliance value in our experiments.)

© 2016 WILEY-VCH Verlag GmbH & Co. KGaA, Weinheim

Furthermore, the SET and RESET of the bilayer junction happens at similar voltages but the initial current can differ by three orders of magnitude. If Joule heating is moving the defects then the SET and RESET should occur at similar power, i.e., very different switching voltages, which is contradictory to the experimental observations.

Other mechanisms for vacancy diffusion are also likely absent in the bilayers. In a good conductor with high current, electron wind can transfer energy to defects and cause their migration. However this mechanism may be absent as the LCMO is a poor conductor and the PBCO barrier limits the current, which is further reduced when the bilayer is at the high resistance state. Recombination-enhanced diffusion[28,29] can enable the diffusion at low temperature and also can cause memristive behavior of oxides,[22,23] but this effect is also unlikely present in the manganite/cuprate bilayers as there is no non-equilibrium concentration of electrons and holes and thus no carrier recombination.

Besides the vacancy migration mechanism, in some ferromagnet/oxide/ferromagnet MTJs, spin–orbit coupling can rotate the direction of the magnetic moment of one of the ferromagnetic layers through voltage-controlled magnetic anisotropy[30] and cause memristive switching[14] with on/off ratio no greater than 10.[31] This mechanism, however, does not explain the present observations, as only one magnetic layer is present in the bilayer samples. The diffusion of Ag into the oxide, which is commonly observed in programmable metallization cells (PMCs aka CBRAMs aka ECM), is also not likely at-play in the current system. In the PCMs, the host materials are amorphous or polycrystalline, which contain voids or low density regions (amorphous) or grain boundaries (polycrystalline), which act as paths for Ag incorporation from the electrode. In contrast, here we are switching a single-crystalline epitaxial film that contains no voids or grain boundaries for Ag incorporation. Therefore, although we cannot definitively rule out the possible role of oxygen vacancies, a new mechanism may be at play.

It has been shown that at the perovskite manganite/cuprate interface, the magnetic moments on the interfacial Mn layer are significantly different from those in bulk manganite. More specifically, at the LCMO/YBCO interface, an MDL can form[18] resulting from the interfacial Mn layer being coupled AFM to the FM LCMO bulk (strongly suppressing double exchange transport through the interface). If such an MDL can be switched on and off in our manganite/cuprate bilayer by an electric field and the states are metastable (metastability in the magnetic states is known to exist in manganites[32]), the junction should also exhibit memristive hysteresis. In **Figure 2** we show schematically how the MDL would affect the transport, where the details of the heterostructure, such as band bending and the transport in PBCO, are neglected, as they do not affect the discussion below. In the low resistance state (LRS), the MDL is absent. The spin of the interfacial layer is FM coupled to the ferromagnetic LCMO bulk as in Figure 2a, allowing the majority-spin electrons in the LCMO to tunnel through the PBCO, as shown in Figure 2b (the light red area shows the additional barrier from the MDL). In this case, the current is large and R is small. In the high resistance state (HRS), the spin of the interfacial layer is AFM coupled with the LCMO bulk (Figure 2c), giving rise to an MDL. This MDL adds an additional tunneling barrier to the transport of majority-spin electrons (Figure 2d), causing lower current and higher R.

To demonstrate that the above mechanism is in fact active in our LCMO/PBCO bilayers, we performed first-principles DFT calculations. In **Figure 3**a, we show the relaxed structure of the LCMO/PBCO interface and highlight the position of the interfacial MnO_2 layer. It can be seen that the layer is polarized, with the Mn atoms displaced toward the PBCO. External biases, as illustrated in Figure 3b,c, can alter the displacements of positively charged Mn atoms. Quantitative results from DFT calculations are presented below in the discussion of the switching mechanism. As will be shown below, DFT calculations confirm that such structural changes are indeed coupled to the change of magnetic ground state of the interfacial Mn layer and thus can switch the MDL on or off and cause the observed memristive hysteresis.

Using DFT calculations, structural relaxations were performed for the PBCO/LCMO bilayer with fixed magnetic coupling between the interfacial Mn layer and the bulk in both the AFM and FM configurations. To capture the subtle structural difference, we used a very tight convergence setting

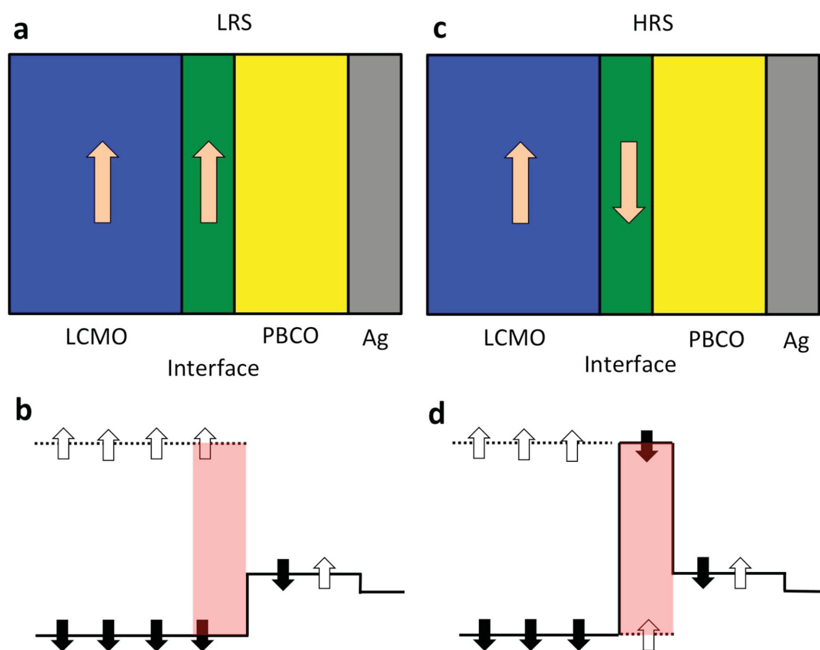

Figure 2. The mechanism of memristive switching at LCMO/PBCO interface. a) The magnetic polarization at LRS, the arrow shows the direction of the magnetic moment. The potential "magnetic dead layer" is marked in green. b) The band diagram of majority (black) and minority (white) spins at LRS. The light red area is the potential additional tunneling barrier if MDL is present. c) The magnetic polarization at HRS. d) The band diagram of majority and minority spins at HRS.

© 2016 WILEY-VCH Verlag GmbH & Co. KGaA, Weinheim

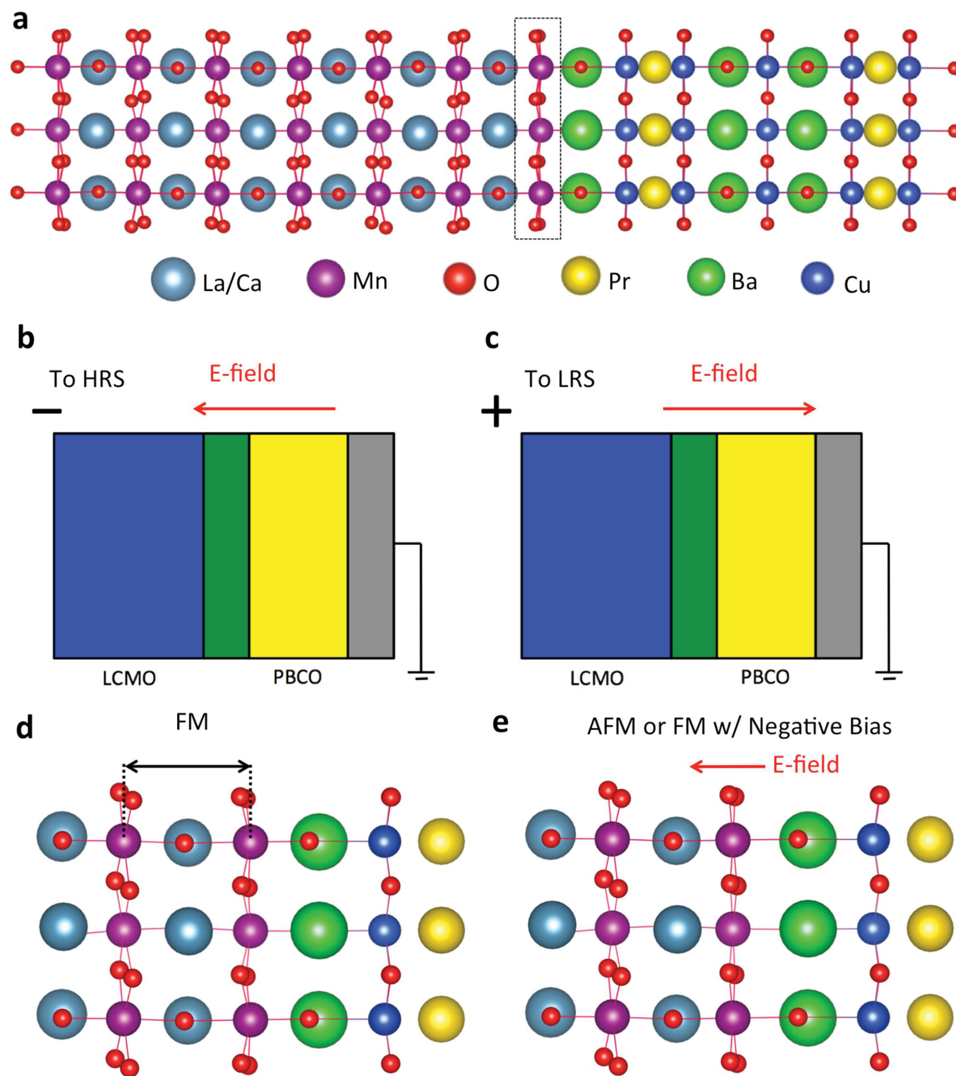

Figure 3. a) The relaxed structure of the LCMO/PBCO interface, projected along a [100] direction of the underlying perovskite lattice. The position of possible "magnetic dead layer" is marked in dotted lines. b, c) The polarities of the applied bias and the directions of the electric field inside the bilayer during the memristive switching. d) The interface layer at optimized geometry when the interfacial Mn atoms are FM-coupled to bulk LCMO. This is also a zoomed-in view of (a). The double-head arrow in black marks the distance between interface Mn layer and the adjacent Mn layer as described in the text. e) An exaggerated illustration of the interface layer at optimized geometry when the interfacial Mn atoms are AFM-coupled to bulk LCMO. It also illustrates the change of Mn displacement from (d) under a negative bias. The change of Mn displacement is magnified by 20 times to 0.2 A for demonstration. The actual change from DFT relaxation is only 0.01 Å as discussed in the text, which is not distinguishable from (d) to the eyes.

that ensures the electronic self-consistency converges to 10^{-6} eV and the forces converge to 10^{-5} eV Å^{-1}. The relaxed structure with FM coupling has an energy 0.5 meV lower than the relaxed structure with AFM coupling, meaning the FM state is the ground state of the bilayer. Therefore, in the resting state, the MDL is not present and the bilayer is at LRS, as shown in Figure 2a,b, consistent with electrical results shown in Figure 1c.

The most important result from the calculations is that the displacements of interfacial Mn atoms are different in the cases of FM and AFM coupled states. In the FM coupled case, the distance between the interfacial Mn layer and the adjacent Mn layer (see Figure 3d) is 3.946 Å; in the AFM coupled case, the value is 3.937 Å. Although the change of 0.01 Å from FM to AFM coupling seems quite small, it is significant when compared to the change of distances between bulk Mn layers from FM to AFM couplings, which do not exceed 0.002 Å. Multiple structural optimizations with different starting geometries were performed to ensure that these results are consistent and are not from artifacts of structural relaxation. Testing structural relaxations was also repeated at different doping levels and with different numerical setups (k-points, plane-wave cutoff) for the DFT calculations. The ≈0.01 Å change in the distance between interfacial and adjacent bulk Mn layers that is much larger than the changes of distances between bulk Mn layers upon changing from FM to AFM coupled states are consistently obtained.

The DFT results on the displacements of interfacial Mn atoms are also consistent with the electrical data shown

 © 2016 WILEY-VCH Verlag GmbH & Co. KGaA, Weinheim

in Figure 1c and the mechanism shown in Figure 2. In the ground state, the Mn ions are displaced toward the PBCO by 3.946 Å from the adjacent Mn layer, as illustrated in Figure 3d. In this state, the interfacial MnO_2 layer is FM coupled to the bulk LCMO, therefore MDL is absent and the bilayer is at LRS. Although the LCMO bulk in the bilayer is nominally metallic at 30% Ca doping,[33] an electric field can be sustained at the interfacial MnO_2 layer because the Thomas–Fermi screening length corresponds to one to two units of LCMO.[34] Furthermore, as discussed below, the properties of the interface LCMO layer differ from those of the bulk and might be viewed as an insulator. A negative bias (Figure 3b) pulls the interfacial Mn toward the LMCO (Figure 3e) and reduces the distance from the adjacent Mn layer. A change of 0.01 Å in the displacements of interfacial Mn layer preconditions the lattice structure to the optimized geometry of the AFM state. DFT calculations were performed to obtain the electronic ground states of the FM and AFM coupled states at the displaced configuration. The results show that the AFM-coupled state has an energy 0.3 meV lower than the FM coupled state. The magnetic moments on the interfacial Mn atoms relax into the AFM coupling state, activating the MDL and switching the bilayer to the HRS. A follow-up positive bias (Figure 3c) pushes the interfacial Mn ions back toward the PBCO. Again, a 0.01 Å change in the displacement preconditions the structure to the optimized geometry of the FM state (Figure 3d). The magnetic moments on the interfacial Mn atoms then relax into the FM coupling state, deactivating the MDL and switching the bilayer back to the LRS. The behavior of MDL in the $La_{0.7}Ca_{0.3}MnO_3/PrBaCu_3O_7$ system and the $La_{0.67}Ca_{0.33}MnO_3/YBaCu_3O_7$ system[18] show that the MDL is a very subtle effect that comes from very small energy difference (around the order of meV) between FM- and AFM-coupled states. In the reported $La_{0.67}Ca_{0.33}MnO_3/YBaCu_3O_7$ system, the AFM state is the ground state and the FM state is metastable, while in in the present $La_{0.7}Ca_{0.3}MnO_3/PrBaCu_3O_7$ system, the FM state is the ground state and the AFM state is metastable.

As mentioned above, a 0.01 Å displacement of the interfacial Mn atoms "preconditions" the geometry of the lattice and facilitates the transition between the magnetic states. The remaining question is whether such displacement can be created by the electric field used in the experiment. Direct calculation of the displacement under the electric field is not feasible due to the complications (doing so would require using a saw-tooth electrostatic potential and periodic replicas of a large supercell containing a bilayer and a vacuum layer, which inevitably has PBCO and LCMO surfaces that would lead to spurious effects) Therefore, we adopted an alternative method: first we use DFT to calculate how much force is needed to create the 0.01 Å displacement, and then compare it to the estimated force from the external electric field. To estimate the forces (and field) required to generate such displacements, we started from the relaxed structure of the FM-coupled state and displaced interface Mn ions toward LCMO by 0.01 Å. DFT calculations were performed for this geometry while keeping the magnetic configuration and other atoms frozen. The calculations show that the forces on the displaced Mn atoms are 0.25 eV $Å^{-1}$, which is the magnitude of the opposite force that needs to be generated by the applied electric field.

Now we estimate the forces exerted on the interfacial Mn ions in the experiment and compare them with those calculated with DFT results. Depending on the level of Ca doping, $La_{1-x}Ca_xMnO_3$ can be a ferromagnetic insulator ($x < 0.2$), a ferromagnetic metal ($0.2 < x < 0.5$), or an anti-ferromagnetic insulator ($0.5 < x$).[33] While the LCMO in our experiment has 30% Ca doping and therefore should be a ferromagnetic metal, the electron density around the Mn atoms at the interface is higher than that in the bulk, which is likely because the local bonding around the interfacial Mn atoms is slightly different from the bulk, as illustrated in Figure 3a. For the interfacial Mn atoms, the calculated average electron density within the Wigner–Seitz cell is 11.574 e, which is greater than the value of 11.546 e for the Mn atoms inside the LCMO part of the bilayer and is close to the calculated value of 11.579 e for pure $LaMnO_3$. Therefore, we assume that the interfacial MnO_2 layer is similar to lightly doped $LaMnO_3$ and thus could be viewed as a ferromagnetic insulator. As a result, when an external bias is applied, the voltage drop is across both the interfacial MnO_2 layer and the PBCO layer. By assigning a thickness of 2 Å to the interface MnO_2 layer (half the spacing between Mn layers) and combining it with the thickness of the PBCO layer (≈8 nm) and the dielectric constants of lightly doped LMO ($\varepsilon = 18$)[35] for the interfacial layer and PBCO ($\varepsilon = 80$),[36] we estimate the electric field at the interface MnO_2 layer to be about 0.02 V $Å^{-1}$. The Born effective charge of interfacial Mn atoms from DFT calculation is 11. Combining these values together, we conclude that an external voltage of 0.5 V generates a force of 0.22 eV $Å^{-1}$ on an interfacial Mn atom. Though this estimate is relatively crude, it is in good agreement with the DFT result that a force of 0.25 eV $Å^{-1}$ is needed to displace the interfacial Mn atom by 0.01 Å and create an MDL.

Now we estimate the on/off resistance ratio of the bilayer, which is the inverse of the transmission coefficient T across the MDL. Using the WKB approximation for a rectangular barrier, T equals $exp\left(-2\sqrt{2m^* V_0/\hbar^2}\, d\right)$, where m^* is the effective mass of electrons in LCMO, V_0 is the barrier height that equals the splitting between spin-up and spin-down electrons, and d is the barrier width. Using $m^* = m_e$,[37] $V_0 = 3.3$ eV,[38] and $d = 3.9$ Å (MnO_2 layer thickness), we obtain $T = 7.5 \times 10^{-4}$ and an on/off ratio of 1.3×10^3, in good agreement with the experimental results shown in Figure 1d,e. The large splitting energy between majority and minority spins in LCMO is an important factor in achieving the high on/off ratio. Other TMO systems would show different on/off ratios upon the creation and elimination of MDL depending on the splitting energy between the majority and minority spins.

In addition to the high on/off ratio, the mechanism described above is in good agreement with several other experimental observations. (1) The DFT calculations are independent of the electrical measurements and predict that negative bias switches the bilayer from the LRS to the HRS and that positive bias switches it from the HRS to the LRS, consistent with the experimental switching directions. (2) Stronger negative bias can cause a more complete formation of the MDL (convert larger portions of the interfacial plane to AFM domains) or make the MDL grow thicker, by propagating it beyond the first interfacial layer, thereby increasing the resistance in the

© 2016 WILEY-VCH Verlag GmbH & Co. KGaA, Weinheim

HRS, as shown in experiments. (3) Meanwhile, once the MDL is destroyed, the bilayer has only one state, thus the resistance in the LRS is the same regardless of the applied positive bias, which is also observed experimentally. (4) The higher external magnetic field can enhance the degree of spin-polarization of injected current that being "analyzed" by the AFM aligned interface plane in the MDL, therefore causing larger resistance in the HRS state, as the experiment shows. (5) The lack of a high on/off ratio in LCMO/PBCO/LCMO trilayer.[20] can be understood as the trilayer has two opposing interfacial Mn layers that are coupled by the magnetic moments in PBCO through the antiferromagnetic interaction between Cu and Mn spins at the interfaces.[20] The calculations we performed confirm the experimental observations that Cu and Mn at the interface are always AFM coupled, regardless of whether Mn atoms at the interface are FM or AFM coupled to Mn in bulk LCMO. In other words, flipping the magnetization of interfacial Mn atoms would cause the flipping of the magnetization of Cu in PBCO. As the two interfacial Mn layers are opposing each other, they cannot be both switched from FM to AFM simultaneously by an electric field that produces displacements in the same direction, because the direction of the displacement that favors AFM coupling in one interface would be "wrong" for the other interface. Therefore, the switching of one side can be suppressed by its coupling to the opposite side through PBCO. The net result is that it is much harder to switch the trilayer and a different mechanism is at play.[20] Indeed, the on/off ratio in a trilayer is only ≈2 while in the bilayer it is about 10^3, which signals different switching mechanisms.

As already mentioned, alternative explanations of the observed switching may be possible. The mechanism described above, however, explains the experimental data and is backed up by first-principles calculations. The physical phenomenon that underlies the memristive switching mechanism shown here is a new type of interfacial magnetoelectricity. It relies on the dependence of the magnetic coupling on the atomic positions, which is in accord with the fact that the magnetic properties in transition metal oxides can be very sensitive to the atomic structures.[39] It bears similarity to the recently observed interfacial magnetoelectricity in magnetic metal/ferroelectric oxide junctions[15–17] where the magnetism at the interface can be controlled by electrically reversing the polarization direction of the ferroelectric. First-principles calculations revealed that in those systems, the change of atomic displacements at the interface upon the switching of the ferroelectric plays the key role in altering the interfacial magnetism.[40] However, even though the magnetic switching in metal/ferroelectric systems only involves the interface, it is necessary to electrically switch the bulk of the ferroelectric. On the contrary, in the LCMO/PBCO bilayer, both magnetic switching and electrical switching are limited to the interface, which potentially offers faster switching and lower energy cost. Using the maximum force 0.25 eV Å^{-1} and the displacement of 0.01 Å, we estimated the energy cost to switching one Mn atom to be 1.3 meV. Therefore, the switching energy of a 10 nm by 10 nm area of the bilayer that represents a "bit" is only 0.8 eV, aka 0.13 atto Joule. In comparison, switching a $BiFeO_3$ ferroelectric memristor[13] with the same area and a thickness of 4.6 nm would require 470 atto Joule at the theoretical limit. Indeed, it takes 0.427 eV to switch one $BiFeO_3$ formula unit[41]). In addition, while the switching in magnetic metal/ferroelectric interfaces involves the change of the in-plane magnetic ordering that has a small effect on spin-current, the switching in LCMO/PBCO bilayer involves the activation of a magnetic "dead" layer, which allows high on/off ratios for applications.

The key factors that enable the type of interfacial magnetoelectricity found in our system are the existence of a polarizable MnO_2 layer at the PBCO/LCMO interface and the modification of the magnetic properties of the Mn atoms by their displacement. As both factors are intrinsic to the perovskite manganite/cuprate interface, these findings should be applicable to other perovskite manganite/cuprate materials systems and possibly other transition metal oxide junctions as well. Further optimization of the materials might result in bilayer junctions with desired electrical properties to be used in a range of applications of memristive devices.[4] One key step would be realizing devices that operate at room temperature. This may be achievable by replacing $LaCaMnO_3$ with $LaSrMnO_3$, whose Curie temperature can be higher than 300 K.[42]

3. Experimental Section

Sample Growth: The samples were grown on top of STO (001) substrates using a high pressure (3.2 mbar) pure oxygen sputtering deposition system at high temperature (900 °C).[19,20] This study fabricated junctions from [PBCO (8 nm)/LCMO 50 nm] bilayers using standard UV optical lithography and ion milling. This study patterned samples into micrometer size (9 × 18 and 5 × 10 μm^2) rectangle shape pillars and measured their magnetotransport properties. For transport properties this study deposited Ag top contacts on the PBCO. Typically 40% of patterned junctions were not shunted and could be measured, which represents a large success ratio of the patterning process. IV curves were measured using current source and voltmeter. For all measurements the top contact was grounded such that negative (positive) voltages corresponded to electric fields pointing downward (upward).

Scanning Transmission Electron Microscopy: HAADF imaging was performed on Nion UltraSTEM 100 and UltraSTEM 200 instruments operated at 100 and 200 kV respectively. Both microscopes use cold field emission electron sources and aberration correctors capable of neutralizing up to fifth order aberrations. Electron energy loss spectroscopy was performed on the Nion UltraSTEM 100 using a Gatan Enfina EEL spectrometer.

DFT Calculations: This study employed the Perdew–Burke–Ernzerhof (PBE)[43] version of the generalized-gradient approximation (GGA) exchange-correlation functional. This study used projector-augmented-wave (PAW) potentials[44] and a plane-wave basis as implemented in the Vienna Ab initio Simulation Package (VASP) code.[45] The kinetic energy cutoff of the plane-wave basis was set to be 368.6 eV. The electronic self-consistent calculations were converged to 10^{-5} eV between two self-consistent steps. The structural relaxations were converged to 10^{-4} eV for the total energy difference between two ionic steps. The simulation cell consisted of a layer of $La_{0.67}C_{0.33}MnO_3$ of 23 Å and a $PrBa_2Cu_3O_7$ layer of 19 Å, with a total of 104 atoms. Brillouin zone sampling was performed by using the 2 × 2 × 1 k-point-mesh. To account for the electron correlations, this study used an implementation[46] of DFT+U methods[47] and applied $U = 2$ eV on Mn 3d orbitals. The 4f electrons on Pr atoms were kept frozen at the core.

Supporting Information

Supporting Information is available from the Wiley Online Library or from the author.

© 2016 WILEY-VCH Verlag GmbH & Co. KGaA, Weinheim

Acknowledgements

X.S., T.J.P., and D.H.-M. contributed equally to this work. The work at Vanderbilt was supported by National Science Foundation grant DMR-1207241, by Department of Energy grant DE-FG02-09ER46554, and by the McMinn Endowment at Vanderbilt University. Computational support was provided by the NSF XSEDE under Grant # TG-DMR130121. Research at UCM was supported by Spanish MICINN through grants MAT2014-52405-C02-01 and Consolider Ingenio 2010—CSD2009-00013 (Imagine), by CAM through grant CAM S2013/MIT-2740. Research at SuperSTEM, the UK National Facility for Aberration-Corrected STEM was supported by the EPSRC. The work at ORNL was partially supported by the Division of Scientific User Facilities of the Office of Basic Energy Sciences, US Department of Energy. Work at Argonne National Laboratory (S.G.E.t.V.) was supported by the U.S. Department of Energy, Office of Science, Materials Science and Engineering Division. Work performed at the Advanced Photon Source was supported by the U.S. Department of Energy, Office of Science, Office of Basic Energy Sciences, under Contract No.DE-AC02-06CH11357. The Advanced Light Source was supported by the Director, Office of Science, Office of Basic Energy Sciences, of the U.S. Department of Energy under Contract No. DE-AC02-05CH11231.

Received: January 31, 2016
Revised: April 19, 2016
Published online: May 27, 2016

[1] L. Chua, *IEEE Trans. Circuit Theory* **1971**, *18*, 507.
[2] Y. V. Pershin, M. Di Ventra, *Adv. Phys.* **2011**, *60*, 145.
[3] S. H. Jo, T. Chang, I. Ebong, B. B. Bhadviya, P. Mazumder, W. Lu, *Nano Lett.* **2010**, *10*, 1297.
[4] J. J. Yang, D. B. Strukov, D. R. Stewart, *Nat. Nanotechnol.* **2013**, *8*, 13.
[5] D. B. Strukov, G. S. Snider, D. R. Stewart, R. S. Williams, *Nature* **2008**, *453*, 80.
[6] A. Asamitsu, Y. Tomioka, H. Kuwahara, Y. Tokura, *Nature* **1997**, *388*, 50.
[7] R. Waser, R. Dittmann, G. Staikov, K. Szot, *Adv. Mater.* **2009**, *21*, 2632.
[8] S. H. Jo, W. Lu, *Nano Lett.* **2008**, *8*, 392.
[9] L. Goux, J. G. Lisoni, X. P. Wang, M. Jurczak, D. J. Wouters, *IEEE Trans. Electron Devices* **2009**, *56*, 2363.
[10] A. S. Blum, J. G. Kushmerick, D. P. Long, C. H. Patterson, J. C. Yang, J. C. Henderson, Y. Yao, J. M. Tour, R. Shashidhar, B. R. Ratna, *Nat. Mater.* **2005**, *4*, 167.
[11] A. Chanthbouala, V. Garcia, R. O. Cherifi, K. Bouzehouane, S. Fusil, X. Moya, S. Xavier, H. Yamada, C. Deranlot, N. D. Mathur, M. Bibes, A. Barthélémy, J. Grollier, *Nat. Mater.* **2012**, *11*, 860.
[12] X. Wang, Y. Chen, H. Xi, H. Li, *IEEE Electron Devices Lett.* **2009**, *30*, 294.
[13] H. Yamada, V. Garcia, S. Fusil, S. Boyn, M. Marinova, A. Gloter, S. Xavier, J. Grollier, E. Jacquet, C. Carrétéro, C. Deranlot, M. Bibes, A. Barthélémy, *ACS Nano* **2013**, *7*, 5385.
[14] W. G. Wang, M. Li, S. Hageman, C. L. Chien, *Nat. Mater.* **2012**, *11*, 64.
[15] Y.-H. Chu, L. W. Martin, M. B. Holcomb, M. Gajek, S.-J. Han, Q. He, N. Balke, C.-H. Yang, D. Lee, W. Hu, Q. Zhan, P.-L. Yang, A. Fraile-Rodríguez, A. Scholl, S. X. Wang, R. Ramesh, *Nat. Mater.* **2008**, *7*, 478.
[16] V. Garcia, M. Bibes, L. Bocher, S. Valencia, F. Kronast, A. Crassous, X. Moya, S. Enouz-Vedrenne, A. Gloter, D. Imhoff, C. Deranlot, N. D. Mathur, S. Fusil, K. Bouzehouane, A. Barthélémy, *Science* **2010**, *327*, 5969.
[17] S. Valencia, A. Crassous, L. Bocher, V. Garcia, X. Moya, R. O. Cherifi, C. Deranlot, K. Bouzehouane, S. Fusil, A. Zobelli, A. Gloter, N. D. Mathur, A. Gaupp, R. Abrudan, F. Radu, A. Barthélémy, M. Bibes, *Nat. Mater.* **2011**, *10*, 753.
[18] W. Luo, S. J. Pennycook, S. T. Pantelides, *Phys. Rev. Lett.* **2008**, *101*, 247204.
[19] M. Varela, Z. Sefrioui, D. Arias, J. Santamaria, *Phys. Rev. Lett.* **1999**, *83*, 3936.
[20] F. A. Cuellar, Y. H. Liu, J. Salafranca, N. Nemes, E. Iborra, G. Sanchez-Santolino, M. Varela, M. G. Hernandez, J. W. Freeland, M. Zhernenkov, M. R. Fitzsimmons, S. Okamoto, S. J. Pennycook, M. Bibes, A. Barthélémy, S. G. E. te Velthuis, Z. Sefrioui, C. Leon, J. Santamaria, *Nat. Commun.* **2014**, *5*, 4215.
[21] J. S. Moodera, T. S. Santos, T. Nagahama, *J. Phys.: Condens. Matter* **2007**, *19*, 165202.
[22] X. Shen, Y. S. Puzyrev, S. T. Pantelides, *MRS Commun.* **2013**, *3*, 167.
[23] X. Shen, K. Yin, Y. S. Puzyrev, Y. Liu, L. Sun, R.-W. Li, S. T. Pantelides, *Adv. Electron. Mater.* **2015**, *1*, 1500019.
[24] Z. W. Xing, N. J. Wu, A. Ignatiev, *Appl. Phys. Lett.* **2007**, *91*, 052106.
[25] D. Strukov, F. Alibart, R. S. Williams, *Appl. Phys. A* **2012**, *107*, 509.
[26] B. Vengalis, V. Lisauskas, V. Pyragas, K. Sliuziene, A. Oginskis, A. Cesnys, J. Santiso, A. Figueras, *J. Phys. IV* **2001**, *11*, 209.
[27] K. H. Warnick, Y. S. Puzyrev, T. Roy, D. M. Fleetwood, R. D. Schrimpf, S. T. Pantelides, *Phys. Rev. B* **2011**, *84*, 214109.
[28] D. V. Lang, *Ann. Rev. Mater. Sci.* **1982**, *12*, 377.
[29] N. Itoh, A. M. Stoneham, *Materials Modification by Electronic Excitation*, Cambridge Univ. Press, Cambridge, UK **2001**.
[30] D. S. Wang, R. Wu, A. J. Freeman, *Phys. Rev. B* **1993**, *47*, 14932.
[31] S. Ikeda, J. Hayakawa, Y. Ashizawa, Y. M. Lee, K. Miura, H. Hasegawa, M. Tsunoda, F. Matsukura, H. Ohno, *Appl. Phys. Lett.* **2008**, *93*, 082508.
[32] Y. Tokura, H. Kuwahara, Y. Moritomo, Y. Tomioka, A. Asamitsu, *Phys. Rev. Lett.* **1996**, *76*, 3186.
[33] P. Schiffer, A. P. Ramirez, W. Bao, S.-W. Cheong, *Phys. Rev. Lett.* **1995**, *75*, 3337.
[34] A. Hoffmann, S. G. E. te Velthuis, Z. Sefrioui, J. Santamaria, M. R. Fitzsimmons, S. Park, M. Varela, *Phys. Rev. B* **2005**, *72*, 140407R.
[35] J. L. Cohn, M. Peterca, J. J. Neumeier, *Phys. Rev. B* **2004**, *70*, 214433.
[36] P. J. Hirst, R. G. Humphreys, in *Handbook of Superconducting Materials Vol. 1* (Eds: D. A. Cardwell, D. S. Ginley), CRC Press, Boca Raton, FL, USA **2003**, p.28.
[37] Y. Liu, F. A. Cuellar, Z. Sefrioui, J. W. Freeland, M. R. Fitzsimmons, C. Leon, J. Santamaria, S. G. E. te. Velthuis, *Phys. Rev. Lett.* **2013**, *111*, 247203.
[38] J. Y. T. Wei, N.-C. Yeh, R. P. Vasquez, A. Gupta, *J. Appl. Phys.* **1998**, *83*, 7366.
[39] J. He, A. Borisevich, S. V. Kalinin, S. J. Pennycook, S. T. Pantelides, *Phys. Rev. Lett.* **2010**, *105*, 227203.
[40] G. Radaelli, D. Petti, E. Plekhanov, I. Fina, P. Torelli, B. R. Salles, M. Cantoni, C. Rinaldi, D. Gutiérrez, G. Panaccione, M. Varela, S. Picozzi, J. Fontcuberta, R. Bertacc, *Nat. Commun.* **2014**, *5*, 3404.
[41] P. Ravindran, R. Vidya, A. Kjekshus, H. Fjellvag, O. Eriksson, *Phys. Rev. B* **2006**, *74*, 224412.
[42] P. Perna, L. Mechin, M. P. Chauvat, P. Ruterana, Ch. Simon, U. Scotti di Uccio, *J. Phys.: Condens. Matter* **2009**, *21*, 306005.
[43] J. P. Perdew, K. Burke, M. Ernzerhof, *Phys. Rev. Lett.* **1996**, *77*, 3865.
[44] G. Kresse, D. Joubert, *Phys. Rev. B* **1999**, *59*, 1758.
[45] G. Kresse, J. Furthmuller, *Phys. Rev. B* **1996**, *54*, 11169.
[46] A. I. Liechtenstein, V. I. Anisimov, J. Zaane, *J. Phys. Rev. B* **1995**, *52*, R5467.
[47] S. L. Dudarev, G. A. Botton, S. Y. Savrasov, C. J. Humphreys, A. P. Sutton, *Phys. Rev. B* **1998**, *57*, 1505.

© 2016 WILEY-VCH Verlag GmbH & Co. KGaA, Weinheim